Materials Horizons

Regio-Specific *N*-Alkyl substitution Tuning the Molecular Packing of High-Performance Non-Fullerene Acceptors

Journal:	*Materials Horizons*
Manuscript ID	MH-COM-07-2021-001127.R3
Article Type:	Communication
Date Submitted by the Author:	20-Sep-2021
Complete List of Authors:	Qi, Feng; City University of Hong Kong, CHEM Jones, Leighton; Northwestern University, Chemistry Jiang, Kui; City University of Hong Kong Jang, Sei-Hum; University of Washington, Department of Chemistry Kaminsky, Werner; University of Washington, Chemistry Oh, Jiyeon; Ulsan National Institute of Science and Technology, Interdisciplinary School of Green Energy Zhang, Hongna; Hong Kong Baptist University, Department of Chemistry Cai, Zongwei; Hong Kong Baptist University, Hong Kong,China, Department of Chemistry Yang, Changduk; Ulsan National Institute of Science and Technology, Interdisciplinary School of Green Energy Kohlstedt, Kevin; Northwestern University, Chemistry Schatz, George; Northwestern University, Chemistry Lin, Francis; City University of Hong Kong, CHEM; University of Washington Department of Chemistry, Marks, Tobin; Northwestern University, Department of Chemistry Jen, Alex; University of Washington, Materials Science and Engineering; University of Washington, Chemistry

New concepts

Non-fullerene acceptors (NFAs) play an important role in the development of highly efficient organic solar cells (OSCs). Benzotriazole (Bz)-based NFAs, in particular, show great potential on achieving high short-circuit current densities with reasonably low energy loss due to their strong photoresponse in the near-infrared (NIR) region and favorable molecular packing that allows efficient charge transport. In this work, four Bz-based NFAs, **mBzS-4F**, **PN6SBO-4F**, **AN6SBO-4F** and **EHN6SEH-4F**, are synthesized through molecularly engineered regio-specific *N*-alkyl substitution and their single-crystal structures systematically characterized for the first time. **AN6SBO-4F** has a long linear *n*-amyl chain on the Bz moiety, leading to non-negligible steric hindrance in its molecular packing. By shortening the *n*-amyl to methyl, **mBzS-4F** shows efficient terminal group interactions and face-to-face π-core interactions. On the other hand, **EHN6SEH-4F** which is *N*-substituted with 2-ethylhexyl chains forms a J-aggregate-like molecular stacking in the out-of-plane direction. OSCs based on PM6:**mBzS-4F** and PM6:**EHN6SEH-4F** show power conversion efficiencies (PCEs) of 17.02% and 17.48%, respectively, which can be attributed to the efficient charge transport through the ordered 3D networks formed from strong intermolecular interactions. This work provides a better understanding of the charge-transporting properties of related NFAs, hence provides a rational design strategy for new solar cell materials via crystal engineering.

Regio-Specific *N*-Alkyl Substitution Tunes the Molecular Packing of High-Performance Non-Fullerene Acceptors

Feng Qi,[a] Leighton O. Jones,[b] Kui Jiang,[c] Sei-Hum Jang,[d] Werner Kaminsky,[e] Jiyeon Oh,[f] Hongna Zhang,[g] Zongwei Cai,[g] Changduk Yang,[f] Kevin L. Kohlstedt,[b] George C. Schatz[b], Francis R. Lin,*[a] Tobin J. Marks,*[b] and Alex K.-Y. Jen*[a,c,d,e,h]

[a]Department of Chemistry, City University of Hong Kong, Kowloon, 999077, Hong Kong. E-mail: alexjen@cityu.edu.hk (A.K.Y.J.); franclin@cityu.edu.hk (F.R.L.)

[b]Department of Chemistry and the Materials Research Center (MRC), Northwestern University, Evanston, Illinois 60208, United States.
E-mail: t-marks@northwestern.edu (T.J.M.)

[c]Department of Materials Science and Engineering, City University of Hong Kong, Kowloon, 999077, Hong Kong.

[d]Department of Materials Science and Engineering, University of Washington, Seattle, Washington 98195-2120, United States.

[e] Department of Chemistry, University of Washington, Seattle, Washington 98195-2120, United States.

[f]Department of Energy Engineering, School of Energy and Chemical Engineering, Perovtronics Research Center, Low Dimensional Carbon Materials Center, Ulsan National Institute of Science and Technology (UNIST), 50 UNIST-gil, Ulju-gun, Ulsan 44919, South Korea.

[g]State Key Laboratory of Environmental and Biological Analysis, Department of Chemistry, Hong Kong Baptist University, Kowloon, 999077, Hong Kong.

[h]Hong Kong Institute for Clean Energy

Abstract

The rapid development of non-fullerene acceptors (NFAs) with strong near-infrared absorption has led to remarkably enhanced short-circuit current densities (J_{scS}) in organic solar cells (OSCs). The NFAs based on benzotriazole (Bz) fused-ring π-core have great potential in delivering both high J_{sc} and decent open-circuit voltage due to their strong intramolecular charge transfer with reasonably low energy loss. In this work, we have designed and synthesized a series of Bz-based NFAs, **PN6SBO-4F**, **AN6SBO-4F** and **EHN6SEH-4F** via regio-specific *N*-alkyl engineering based on the high-performance **mBzS-4F** that was reported previously. The molecular packing of **mBzS-4F**, **AN6SBO-4F**, and **EHN6SEH-4F** single crystals were analyzed by X-ray crystallography in order to provide a comprehensive understanding of the correlation between molecular structure, charge-transporting properties, and solar cell performances. Compared with the typical honeycomb single-crystal structure of Y6 derivatives, these NFAs exhibit distinctly different molecular packing patterns. The strong interactions of terminal indanone groups in **mBzS-4F** and J-aggregate-like packing in **EHN6SEH-4F** lead to the formation of ordered 3D networks in single-crystals with channels for efficient charge transport. Consequently, OSCs based on **mBzS-4F** and **EHN6SEH-4F** show efficient photo-to-current conversions, achieving a highest power conversion efficiency of 17.48% with a J_{sc}=28.83 mA/cm^2.

New concepts

Non-fullerene acceptors (NFAs) play an important role in the development of highly efficient organic solar cells (OSCs). Benzotriazole (Bz)-based NFAs, in particular, show great potential on achieving high short-circuit current densities with reasonably low energy loss due to their strong photoresponse in the near-infrared (NIR) region and favorable molecular packing that allows efficient charge transport. In this work, four Bz-based NFAs, **mBzS-4F**, **PN6SBO-4F**, **AN6SBO-4F** and **EHN6SEH-4F**, are synthesized through molecularly engineered regio-specific *N*-alkyl substitution and their single-crystal structures systematically characterized for the first time. **AN6SBO-4F** has a long linear *n*-amyl chain on the Bz moiety, leading to non-negligible steric hindrance in its molecular packing. By shortening the *n*-amyl to methyl, **mBzS-4F** shows efficient terminal group interactions and face-to-face π-core interactions. On the other hand, **EHN6SEH-4F** which is *N*-substituted with 2-ethylhexyl chains forms a J-aggregate-like molecular stacking in the out-of-plane direction. OSCs based on PM6:**mBzS-4F** and PM6:**EHN6SEH-4F** show power conversion efficiencies (PCEs) of 17.02% and 17.48%, respectively, which can be attributed to the efficient charge transport through the ordered 3D networks formed from strong intermolecular interactions. This work provides a better understanding of the charge-transporting properties of related NFAs, hence provides a rational design strategy for new solar cell materials via crystal engineering.

Introduction

New renewable energy technologies that can lower the demand for fossil fuels have received increasing attention recently. Among those that have been actively pursued, organic solar cells (OSCs) offer the attraction of being light weight, solution-processable and , composed of earth-abundant materials, and readily manufactured by solution-based printing techniques, making them a very attractive candidate.[1-7] Currently, the power conversion efficiency (PCE) of OSCs have already achieved over 18%[8, 9] due to the vigorous development of non-fullerene acceptors (NFAs) which have extended absorption to the near-infrared (NIR) region, yielding dramatically enhanced short-circuit current densities (J_{scS}).[10-16]

Among the NFA classes developed, Y6 and its derivatives have been the most investigated because of the remarkable OSC PCEs achieved via the closely stacked crescent-shaped molecular geometries with the electron-withdrawing benzo[2,1,3]thiadiazole (BT), fused into the core of the molecular skeleton.[17] Several studies have been reported to illustrate the high performance of Y6-based OSCs from the perspective of crystal engineering.[18-21] Yip *et al.* studied the relationship between the Y6 crystal structure and performance of the OSCs, explaining the existence of unique molecular stacking in both single-crystal and films, which benefits the exciton delocalization and results in efficient charge generation.[22] Previously, this laboratory also reported a selenium-substituted Y6 derivative, CH1007, demonstrating strong π-core interactions similar to that of Y6 in their single-crystals, which enhanced the charge transport and PCE.[23] Furthermore, CH1007 possesses two selenophene units with stronger electron-donating properties in the π-core compared to Y6, which led to red-shifted absorption and enhanced J_{sc}.

In contrast, compared with the BT unit in Y6, benzotriazole (Bz) is a weaker electron-withdrawing unit making the π-core slightly more electron-rich than Y6, which should not only can further extend the NIR absorption due to stronger intramolecular charge transfer (ICT), but also retain similar low energy loss like Y6.[24-26] Wu *et al.* reported a Bz-based NFA, Y11, possessing a narrow bandgap of 1.31 eV that yielded a PCE of 16.54% with a high J_{sc} of 26.74 mA/cm^2 and a non-radiative recombination energy loss of 0.17 eV.[27] This laboratory also

designed and synthesized a Bz-based, Se-substituted fused-ring π-core BzS and two NIR-absorbing NFAs, **mBzS-4F** and **EHBzS-4F**, both with bandgaps below 1.25 eV.[28] The **mBzS-4F**-based devices exhibited a high J_{sc} of 27.72 mA/cm^2, leading to a PCE of 17.02% with a reasonably small energy loss of 0.446 eV, demonstrating the potential to simultaneously obtain high J_{sc} and low energy loss in OSCs with Bz-based NFAs.

However, the molecular packing of Bz-based NFAs has not been systematically characterized in the context of crystal engineering strategies. Furthermore, side-chain engineering is also a useful strategy to fine-tune the thin-film morphology.[29-33] Sun *et al.* synthesized a series of Y6 derivatives flanked with branched side-chains, showing that molecular packing is significantly affected by different alkyl chain lengths.[34] The L8-BO-based OSCs exhibit a high PCE of 18.32%, which can be attributed to the improved charge transport due to enhanced structural order arising from the engineered side-chains.

Compared with BT-based Y6 derivatives, the Bz-based NFAs have an additional site for *N*-alkyl substitution on the Bz moiety. In this work, the length of linear *N*-alkyl groups on Bz moiety is systematically altered with methyl, *n*-propyl, and *n*-amyl groups while the same 2-butyloctyl group was retained as the *N*-alkyl substituent on the pyrrole units (**Fig. 1**). It is also noteworthy that our previously demonstrated NFA, EHBzS-4F, substituted with 2-ethylhexyl on Bz unit and 2-butyloctyl on pyrrole units, has good solubility but lower crystallinity.[28] Therefore, the long 2-butyloctyl was replaced with shorter 2-ethylhexyl on the pyrrole units, aiming at enhancing the crystallinity while maintaining sufficient solubility for processing. The synthetic routes are shown in **Schemes S1** & **S2**. After different *N*-alkyl-substituted central cores were formylated and condensed with the terminal groups, to yield **PN6SBO-4F**, **AN6SBO-4F** and **EHN6SEH-4F**. Diffraction-quality single-crystals of **AN6SBO-4F**, **EHN6SEH-4F** and the previously reported **mBzS-4F** were successfully grown to investigate their solid-state structures. The molecular packing of Bz-based NFAs is systematically compared for the first time in the perspective of crystal engineering strategies.

After carefully analyzing the single-crystal structures, we find distinctly different packing patterns for this series of Bz-based NFAs compared with the typical honeycomb network

observed in Y6. **AN6SBO-4F** possesses a longer linear *n*-amyl chain on Bz moiety which induces more disordered packing and larger distances between neighboring molecules. By shortening the *n*-amyl to methyl, quite efficient terminal group interactions and face-to-face π-core interactions are created in the **mBzS-4F** unit cell. In contrast, **EHN6SEH-4F** crystallizes with pronounced J-aggregate-like packing patterns formed by the π-π stacking between the terminal groups in the out-of-plane direction, leading to a highly ordered 3D network. This suggests that **mBzS-4F** and **EHN6SEH-4F** should be more efficient in charge transport. OSCs based on PM6:**mBzS-4F** deliver a PCE of 17.02% with a J_{sc} of 27.72 mA/cm^2 and FF of 76.35%, while that of PM6:**EHN6SEH-4F** also exhibits a high J_{sc} of 28.83 mA/cm^2 and FF of 74.64%, resulting in a PCE of 17.48% in accordance with the analysis.

Results and Discussion

Figs. 2a and **2b** show the solution and thin-film UV-Vis absorption spectra of the present NFAs, and their optical properties are summarized in **Table S1**. In dilute solution of $CHCl_3$, all four acceptors show similar absorption profiles with a maximum peak at ~770 nm. In thin-films, the main absorption peaks of **mBzS-4F**, **PN6SBO-4F**, **AN6SBO-4F** and **EHN6SEH-4F** have a characteristic red-shift of ~100 nm. Moreover, **mBzS-4F** has a stronger absorbance than the others in the high photon energy range, showing two distinct 0-1 and 0-2 transition peaks that imply a more ordered microstructure.[35] The optical bandgaps were calculated by the absorption onset obtained from the thin-films, and are 1.25, 1.28, 1.27 and 1.29 eV for **mBzS-4F**, **PN6SBO-4F**, **AN6SBO-4F** and **EHN6SEH-4F**, respectively. Such low NFA bandgaps can be a benefit in enhancing J_{sc}.

The electrochemical properties of NFAs were measured using cyclic voltammetry. The highest occupied molecular orbital (HOMO) and the lowest unoccupied molecular orbital (LUMO) levels were derived by the onset of oxidation and reduction potentials (**Fig. S1**). As shown in **Fig. 2c**, the HOMO/LUMO energy levels of **mBzS-4F**, **PN6SBO-4F**, **AN6SBO-4F** and **EHN6SEH-4F** were calculated to be -5.61/-3.92, -5.63/-3.87, -5.60/-3.88 and -5.59/-3.89 eV, respectively.

Molecular packing has a great influence on OSC charge transporting properties.[36-38]

Therefore, a single-crystal X-ray diffraction study was performed to provide comprehensive insight into the molecular self-assembly in solid state. Diffraction-quality single-crystals of **mBzS-4F**, **AN6SBO-4F**, and **EHN6SEH-4F** were grown by slow diffusion in a ternary solvent system, and the diffraction data were collected at -173 ^{o}C on a single crystal X-ray diffractometer with Mo-radiation (**Table S2-S4**). The single-crystal structures are shown in **Fig. 3** and the crystal parameters are summarized in **Table 1**. Besides, the ORTEP view of all single-crystal structures are shown in **Fig. S2**. All three NFAs show an intramolecular Se-O distance shorter than 2.70 Å (**Fig. 3a-c**), suggesting an efficient intramolecular non-covalent interaction that helps form conformational locks between π-core and terminal groups.[39, 40]

Due to the twisted π-core and the special crescent-shaped molecular geometry, enantiomers are formed in the present crystals. Thus, **mBzS-4F** displays as a complicated enantiomeric mixture, having three pairs of *M*/*P*, *M*′/*P*′, and *M*″/*P*″ enantiomers with π-core torsion angles of 13.8(8)°, 11.9(8)° and 16.6(5)°, respectively (**Fig. 3d**). This special packing may be caused by the comparatively large twist of the π-core. In addition, coplanarity was also computed between the π-core and flanking terminal groups. The D-A dihedral angles of **mBzS-4F** are 3.3(5)°/3.5(9)°, 1.1(0)°/2.9(9)° and 1.7(2)°/2.8(2)° for *M*/*P*, *M*′/*P*′, and *M*″/*P*″ enantiomers, respectively. **EHN6SEH-4F** possesses a pair of *M*/*P* enantiomers, with a π-core torsion of 8.6(7)° and D-A dihedral angles of 3.3(9)°/3.9(3)° (**Fig. 3e**). Compared to **mBzS-4F** and **EHN6SEH-4F**, **AN6SBO-4F** also has a pair of *M*/*P* enantiomers corresponding to a π-core torsion of 4.2(2)° and D-A dihedral angles of 3.3(9)°/18.7(0)° (**Fig. 3f**). We also measured the π−π distances between the closely packed molecules. In **EHN6SEH-4F**, a π−π distance of 3.40(5) Å was measured between two parallel planes defined by the selenophene moieties on adjacent molecules. In **AN6SBO-4F**, the π-π distance was measured between two planes of the five-membered ring of indanone moiety as 3.31(6) Å. All enantiomers of **mBzS-4F** have substantial π-core torsion, where a set of parallel planes for determining π-π distance is not found. Furthermore, π-core interactions can be observed in **mBzS-4F** and **AN6SBO-4F** (**Fig. S3**). This type of π-π stacking of Bz units was reported in literature before.[41] The π-core interaction distance in **mBzS-4F** is 3.44(4) and 3.56(4) Å, which is larger than that (3.19(6) Å)

of **AN6SBO-4F**. This can be attributed to the larger π-core torsion of **mBzS-4F**.

In the literature,[19, 23] Y6 has ordered molecular packing enabled by two distinct terminal group interactions and a unique face-to-face π-core interaction between the BT unit with S… N interaction in the adjacent molecules, eventually forming a honeycomb-shaped 3D network. However, **mBzS-4F**, **AN6SBO-4F** and **EHN6SEH-4F** show different packing patterns. Top views of the molecular packing of **mBzS-4F**, **AN6SBO-4F** and **EHN6SEH-4F** are shown in **Fig. 3g-i**. The *N*-alkyl groups on Bz moiety were not omitted to show their influence on molecular packing. It was found that longer *N*-alkyl groups on Bz moiety push away the adjacent molecules, and weaken the face-to-face π-core interaction between the head-to-head Bz moieties. The specific long-range order of the crystals is shown in **Fig. S4**. Note that all crystals have a molecular packing in an oblique direction across the crystal lattice. Although **mBzS-4F** has some disorder in the molecular packing, it still maintains efficient terminal group interactions and face-to-face π-core interactions owing to its shortest *N*-methyl group. However, the linear and longer *n*-amyl group in **AN6SBO-4F** interferes with the molecular packing, leading to disordered packing in the out-of-plane direction, which may undermine the charge transport.

Compared with **mBzS-4F** and **AN6SBO-4F**, the π-core interaction is not well developed in **EHN6SEH-4F** due to the long and branched *N*-alkyl group on the Bz moiety. However, it exhibits J-aggregate-like packing patterns between the terminal groups in adjacent molecules, which correlate with the reduced length of *N*-alkyl on pyrrole unit and reduced steric hindrance compared to **mBzS-4F** and **EHN6SEH-4F**, promoting the formation of a 3D network. This can promote exciton diffusion and improve charge carrier generation,[42, 43] thereby enhancing J_{sc}.

To further investigate the intermolecular interactions in the NFAs, grazing-incidence wide-angle X-ray scattering (GIWAXS) analysis was performed. The 2D GIWAXS patterns and the extracted 1D profiles are shown in **Fig. S5**. All the NFAs show preferred face-on orientations with a clear π-π diffraction peak in the out-of-plane (OOP) direction at ~1.7 $Å^{-1}$ and a lamellar (100) peak at ~0.4 $Å^{-1}$ in the in-plane (IP) direction (**Table S5**). This indicates all NFAs studied

have pronounced π–π stacking beneficial for charge transport. Additionally, the space-charge-limited-current (SCLC) electron mobility measurement was also performed (**Fig. S6**). The electron mobility of **EHN6SEH-4F** is 1.4×10^{-4} $cm^2/V\cdot s$, which is higher than those (9.2×10^{-5} and 8.0×10^{-5} $cm^2/V\cdot s$) of **PN6SBO-4F** and **EHN6SEH-4F** (**Table S6**). **mBzS-4F** also has a high electron mobility of 2.8×10^{-4} $cm^2/V\cdot s$. These results are consistent with the observed molecular packing.

The intermolecular electronic coupling was also computed to provide better understanding of the charge-transporting properties of these NFAs. Firstly, a reference molecule was chosen in the single crystal and labeled as A, then its close neighbors were labeled as B, C, ..., *etc.* (**Fig. 4a**). **mBzS-4F** has 7 neighboring molecules around the reference, which is more than that (4) of **AN6SBO-4F.** The longer *n*-amyl on the Bz unit and more twisted D-A dihedral angles of **AN6SBO-4F** reduce the overall coplanarity of the molecule, leading to a less ordered single-crystal packing, and thus fewer intermolecular contacts. In contrast, **EHN6SEH-4F** has 9 neighbors around the reference due to its special packing mode in the oblique direction, leading to an extended intermolecular network. The electronic coupling was calculated by density functional theory (DFT) according to the reported method.[44, 45] **Fig. 4b** shows the couplings of the three acceptors and the detailed values are summarized in **Tables S7-S9**. It is found that **mBzS-4F** has two large couplings, $|J|_{AE}$ = 22.2 meV and $|J|_{AF}$ = 37.4 meV, due to the efficient interactions between terminal groups and π-cores. In comparison, large couplings of $|J|_{AD}$ = 17.4 meV and $|J|_{AE}$ = 45.2 meV were also found in **AN6SBO-4F** resulting from the J-aggregate-like packing of dimers. The four large couplings of $|J|$ = (12.5 (AB), 19.3 (AC), 19.3 (AG), and 20.3 (AH) meV) in **EHN6SEH-4F** show that the reference molecule possesses strong interactions with adjacent molecules, and further forms a long-range channel through extension of ordered π-π stacking in the single-crystal. A stronger degree of overlapping between adjacent molecules not only leads to a higher degree of electronic coupling, but also significantly aids the dissociation of photo-generated excitons and the generation of free charge carriers.[22, 46] Furthermore, long-range order in NFA packing enhances the charge transport resulting in more efficient photo-to-current conversion.

The photovoltaic performance of the PM6:NFA-based OSCs was investigated by fabricating conventional OSCs with an architecture of ITO/PEDOT:PSS/PM6:NFAs/PNDIT-F3N/Ag. The current density-voltage (*J-V*) plots are shown in **Fig. 5a** and the performance parameters are summarized in **Table 2**. The PM6:**mBzS-4F**- and PM6:**EHN6SEH-4F**-based OSCs all exhibit high J_{scS} of 27.72 and 28.83 mA/cm^2, respectively, with a similar open-circuit voltages (V_{oc}) of ~0.80 V for both, resulting in high PCEs of 17.02% and 17.48%. Meanwhile, these devices also showed higher fill factors (FF) of 76.35% and 74.64%. This may result from the ordered molecular packing that leads to efficient charge transport. In contrast, the devices based on PM6:**PN6SBO-4F** deliver a PCE of only 12.73% with a V_{oc} of 0.825 V, J_{sc} of 23.13 mA/cm^2, and FF of 66.65%. In addition, the PM6:**AN6SBO-4F**-based devices exhibit a V_{oc} of 0.822 V, J_{sc} of 16.06 mA/cm^2, FF of 62.98%, and a low PCE of 8.32%. Compared with Y6-based OSCs, all the devices show slightly lower V_{oc} values which can be attributed to reduced NFA bandgap according to the energy gap law.[47] The poor J_{sc} and FF can be attributed to the lack of long-range channel with ordered π-π stacking as observed in the crystal structure of **AN6SBO-4F**. To further investigate the relationship between the blend morphology and the photovoltaic performance, atomic force microscopy (AFM) was employed. The mean-square surface roughness (R_q) of PM6:**mBzS-4F**, PM6:**PN6SBO-4F**, PM6:**AN6SBO-4F**, and PM6:**EHN6SEH-4F** blends films are 0.93, 3.09, 2.86 and 0.86 nm, respectively (**Fig. S7**). The rougher surface in PM6:**PN6SBO-4F** and PM6:**ANSBO-4F** films may lead to unfavorable charge transport properties and serious recombination, resulting in lower J_{sc} and FF.[48-50]

To further investigate the photoresponse of devices based on PM6:NFAs, external quantum efficiency (EQE) spectra were collected (**Fig. 5b**). The PM6:**mBzS-4F**-based devices show efficient charge generation in the region of 465-875 nm with EQEs over 70%. The devices based on PM6:**EHN6SEH-4F** also exhibit a broad photoresponse from 460 to 900 nm with the EQE value above 70%. However, the PM6:**PN6SBO-4F**- and PM6:**AN6SBO-4F**-based devices display relatively weak photoresponses. This may be due to the disordered molecular packing caused by their long *N*-alkyl groups on Bz moiety. Note that the integrated photocurrent densities of the PM6:**mBzS-4F**-, PM6:**PN6SBO-4F**-, PM6:**AN6SBO-4F**-, and

PM6:**EHBzS-4F**-based devices are 27.17, 22.21, 15.20 and 27.80 mA/cm^2, respectively, which agree well with J_{sc} extracted from the *J*-*V* plots.

Conclusions

We have designed and synthesized a series of NIR-absorbing Bz-based NFAs, **mBzS-4F**, **PN6SBO-4F**, **AN6SBO-4F** and **EHN6SEH-4F**, by introducing various linear *N*-alkyl groups (methyl, *n*-propyl, and *n*-amyl) and branched *N*-alkyl groups (2-ethylhexyl and 2-butyloctyl) onto the Bz and pyrrole moieties on the NFA π-cores. All NFAs show a bandgap below 1.30 eV, resulting from the enhanced ICT due to more electron-rich central π-core than that of Y6. For the first time, diffraction-quality single-crystals of Bz-based NFAs were grown and systematically investigated to study the influence of different *N*-alkyl groups on the solid-state intermolecular interactions. Efficient terminal group interactions and face-to-face π-core interactions are maintained in **mBzS-4F** possessing the shortest *N*-methyl alkyl group on the Bz moiety. Although the π-core interaction in **EHN6SEH-4F** has completely disappeared due to its longer *N*-alkyl on the Bz moiety, it still forms efficient charge transport channels induced by the strong intermolecular interactions of terminal groups between adjacent molecules. This enables J-aggregate-like stacking and a 3D network. However, the longer linear *n*-amyl on the Bz moiety of **AN6SBO-4F** results in poor long-range order in molecular packing, which undermines the charge transport. Consequently, the PM6:**mBzS-4F**- and PM6:**EHN6SEH-4F**-based OSCs exhibit high J_{sc} of 27.72 and 28.83 mA/cm^2, respectively, resulting in high PCEs of 17.02% and 17.48%. On the contrary, the devices based on PM6:**PN6SBO-4F** and PM6:**AN6SBO-4F** only delivers PCEs of 12.73% and 8.32%, respectively. This work provides a better understanding of the charge- transporting properties of related NFAs and a rational molecular design strategy for creating new high-efficiency OSC materials via crystal engineering.

Conflicts of interest

There are no conflicts to declare.

Acknowledgements

A.K.Y.J. thanks the sponsorship of the Lee Shau-Kee Chair Professor (Materials Science), and the support from the APRC Grant of the City University of Hong Kong (9380086), Innovation and Technology Fund (ITS/497/18FP, GHP/021/18SZ), the US Office of Naval Research (N00014-20-1-2191), the GRF grant (11307621) and the CRF grant (C6023-19GF) from the Research Grants Council of Hong Kong, Guangdong Major Project of Basic and Applied Basic Research (2019B030302007), Guangdong-Hong Kong-Macao Joint Laboratory of Optoelectronic and Magnetic Functional Materials (2019B121205002). L.O.J., K.L.K., G.C.S. and T.J.M. acknowledge the support from the Center for Light Energy Activated Redox Processes (LEAP), an Energy Frontier Research Center funded by the U.S. Department of Energy, Office of Science, Office of Basic Energy Sciences, under Award #DE-SC0001059. T.J.M. acknowledges the US Office of Naval Research (N00014-20-1-2116). The authors also thank Dr. Qunping Fan from the City University of Hong Kong and Dr. Shanshan Chen from Chongqing University for their helps to make this work more complete.

Notes and references

1. C. Yan, S. Barlow, Z. Wang, H. Yan, A. K.-Y. Jen, S. R. Marder and X. Zhan, *Nat. Rev. Mater.,* 2018, **3**, 18003-18021.
2. W. Xu and F. Gao, *Mater. Horiz.*, 2018, **5**, 206-221.
3. Y. Lin, J. Wang, Z. G. Zhang, H. Bai, Y. Li, D. Zhu and X. Zhan, *Adv. Mater.*, 2015, **27**, 1170-1174.
4. Q. Fan, H. Fu, Q. Wu, Z. Wu, F. Lin, Z. Zhu, J. Min, H. Y. Woo and A. K.-Y. Jen, *Angew. Chem. Int. Ed.*, 2021, **60**, 15935–15943.
5. F. Lin, L. Zuo, K. Gao, M. Zhang, S. B. Jo, F. Liu and A. K.-Y. Jen, *Chem. Mater.*, 2019, **31**, 6770-6778.
6. Y. Cui, H. Yao, J. Zhang, T. Zhang, Y. Wang, L. Hong, K. Xian, B. Xu, S. Zhang, J. Peng, Z. Wei, F. Gao and J. Hou, *Nat. Commun.*, 2019, **10**, 2515-2522.
7. F. Qi, Y. Zhang, M. Wan, J. Liu and L. Huo, *J. Mater. Chem. C*, 2018, **6**, 4208-4216.

8. L. Zhan, S. Li, X. Xia, Y. Li, X. Lu, L. Zuo, M. Shi and H. Chen, *Adv. Mater.*, 2021, **33**, 2007231.

9. Q. Liu, Y. Jiang, K. Jin, J. Qin, J. Xu, W. Li, J. Xiong, J. Liu, Z. Xiao, K. Sun, S. Yang, X. Zhang and L. Ding, *Sci. Bull.*, 2020, **65**, 272-275.

10. W. Gao, H. Fu, Y. Li, F. Lin, R. Sun, Z. Wu, X. Wu, C. Zhong, J. Min, J. Luo, H. Y. Woo, Z. Zhu and A. K.-Y. Jen, *Adv. Energy Mater.*, 2020, **11**, 2003177.

11. K. Jiang, Q. Wei, J. Y. L. Lai, Z. Peng, H. K. Kim, J. Yuan, L. Ye, H. Ade, Y. Zou and H. Yan, *Joule*, 2019, **3**, 3020-3033.

12. Y. Chang, T.-K. Lau, M.-A. Pan, X. Lu, H. Yan and C. Zhan, *Mater. Horiz.*, 2019, **6**, 2094-2102.

13. Z. Yao, X. Liao, K. Gao, F. Lin, X. Xu, X. Shi, L. Zuo, F. Liu, Y. Chen and A. K.-Y. Jen, *J. Am. Chem. Soc.*, 2018, **140**, 2054-2057.

14. H. Fu, W. Gao, Y. Li, F. Lin, X. Wu, J. H. Son, J. Luo, H. Y. Woo, Z. Zhu and A. K.-Y. Jen, *Small Methods*, 2020, **4,** 2000687.

15. W. Gao, B. Fan, F. Qi, F. Lin, R. Sun, X. Xia, J. Gao, C. Zhong, X. Lu, J. Min, F. Zhang, Z. Zhu, J. Luo and A. K.-Y. Jen, *Adv. Funct. Mater.*, 2021, DOI: 10.1002/adfm.202104369.

16. S. Li, L. Zhan, Y. Jin, G. Zhou, T. K. Lau, R. Qin, M. Shi, C. Z. Li, H. Zhu, X. Lu, F. Zhang and H. Chen, *Adv. Mater.*, 2020, **32**, 2001160.

17. J. Yuan, Y. Zhang, L. Zhou, G. Zhang, H.-L. Yip, T.-K. Lau, X. Lu, C. Zhu, H. Peng, P. A. Johnson, M. Leclerc, Y. Cao, J. Ulanski, Y. Li and Y. Zou, *Joule*, 2019, **3**, 1140-1151.

18. H. Chen, H. Lai, Z. Chen, Y. Zhu, H. Wang, L. Han, Y. Zhang and F. He, *Angew. Chem. Int. Ed.*, 2020, **60**,3238-3246.

19. L. Zhu, M. Zhang, G. Zhou, T. Hao, J. Xu, J. Wang, C. Qiu, N. Prine, J. Ali, W. Feng, X. Gu, Z. Ma, Z. Tang, H. Zhu, L. Ying, Y. Zhang and F. Liu, *Adv. Energy Mater.*, 2020, **10**, 1904234.

20. W. Zhu, A. P. Spencer, S. Mukherjee, J. M. Alzola, V. K. Sangwan, S. H. Amsterdam,

S. M. Swick, L. O. Jones, M. C. Heiber, A. A. Herzing, G. Li, C. L. Stern, D. M. DeLongchamp, K. L. Kohlstedt, M. C. Hersam, G. C. Schatz, M. R. Wasielewski, L. X. Chen, A. Facchetti and T. J. Marks, *J. Am. Chem. Soc.*, 2020, **142**, 14532-14547.

21. X. Li, I. Angunawela, Y. Chang, J. Zhou, H. Huang, L. Zhong, A. Liebman-Peláez, C. Zhu, L. Meng, Z. Xie, H. Ade, H. Yan and Y. Li, *Energy Environ. Sci.*, 2020, **13**, 5028-5038.
22. G. Zhang, X.-K. Chen, J. Xiao, P. C. Y. Chow, M. Ren, G. Kupgan, X. Jiao, C. C. S. Chan, X. Du, R. Xia, Z. Chen, J. Yuan, Y. Zhang, S. Zhang, Y. Liu, Y. Zou, H. Yan, K. S. Wong, V. Coropceanu, N. Li, C. J. Brabec, J.-L. Bredas, H.-L. Yip and Y. Cao, *Nat. Commun.*, 2020, **11,** 3943-3952.
23. F. Lin, K. Jiang, W. Kaminsky, Z. Zhu and A. K.-Y. Jen, *J. Am. Chem. Soc.*, 2020, **142**, 15246-15251.
24. J. Yuan, T. Huang, P. Cheng, Y. Zou, H. Zhang, J. L. Yang, S. Y. Chang, Z. Zhang, W. Huang, R. Wang, D. Meng, F. Gao and Y. Yang, *Nat. Commun.*, 2019, **10**, 570-577.
25. R. Wang, J. Yuan, R. Wang, G. Han, T. Huang, W. Huang, J. Xue, H. C. Wang, C. Zhang, C. Zhu, P. Cheng, D. Meng, Y. Yi, K. H. Wei, Y. Zou and Y. Yang, *Adv. Mater.*, 2019, **31**, 1904215.
26. C. Zhu, J. Yuan, F. cai, L. Meng, H. Zhang, H. Chen, J. Li, B. Qiu, H. Peng, S. Chen, Y. Hu, C. Yang, F. Gao, Y. Zou and Y. Li, *Energy Environ. Sci.*, 2020, **13**, 2459-2466.
27. S. Liu, J. Yuan, W. Deng, M. Luo, Y. Xie, Q. Liang, Y. Zou, Z. He, H. Wu and Y. Cao, *Nat. Photonics*, 2020, **14**, 300-305.
28. F. Qi, K. Jiang, F. Lin, Z. Wu, H. Zhang, W. Gao, Y. Li, Z. Cai, H. Y. Woo, Z. Zhu and A. K.-Y. Jen, *ACS Energy Lett.*, 2021, **6**, 9-15.
29. Y. Cui, H. Yao, J. Zhang, K. Xian, T. Zhang, L. Hong, Y. Wang, Y. Xu, K. Ma, C. An, C. He, Z. Wei, F. Gao and J. Hou, *Adv. Mater.*, 2020, **32**, 1908205.
30. G. Chai, Y. Chang, J. Zhang, X. Xu, L. Yu, X. Zou, X. Li, Y. Chen, S. Luo, B. Liu, F. Bai, Z. Luo, H. Yu, J. Liang, T. Liu, K. S. Wong, H. Zhou, Q. Peng and H. Yan, *Energy Environ. Sci.*, 2021, **14**, 3469-3479.

31. T. Liu, L. Huo, S. Chandrabose, K. Chen, G. Han, F. Qi, X. Meng, D. Xie, W. Ma, Y. Yi, J. M. Hodgkiss, F. Liu, J. Wang, C. Yang and Y. Sun, *Adv. Mater.*, 2018, **30**, 1707353.

32. L. Huo, X. Xue, T. Liu, W. Xiong, F. Qi, B. Fan, D. Xie, F. Liu, C. Yang and Y. Sun, *Chem. Mater.*, 2018, **30**, 3294-3300.

33. I. Meager, R. S. Ashraf, S. Mollinger, B. C. Schroeder, H. Bronstein, D. Beatrup, M. S. Vezie, T. Kirchartz, A. Salleo, J. Nelson and I. McCulloch, *J. Am. Chem. Soc.*, 2013, **135**, 11537-11540.

34. C. Li, J. Zhou, J. Song, J. Xu, H. Zhang, X. Zhang, J. Guo, L. Zhu, D. Wei, G. Han, J. Min, Y. Zhang, Z. Xie, Y. Yi, H. Yan, F. Gao, F. Liu and Y. Sun, *Nat. Energy*, 2021, **6**, 605–613.

35. R. C. Coffin, J. Peet, J. Rogers and G. C. Bazan, *Nat. Chem.*, 2009, **1**, 657-661.

36. Y. Tsutsui, G. Schweicher, B. Chattopadhyay, T. Sakurai, J. B. Arlin, C. Ruzie, A. Aliev, A. Ciesielski, S. Colella, A. R. Kennedy, V. Lemaur, Y. Olivier, R. Hadji, L. Sanguinet, F. Castet, S. Osella, D. Dudenko, D. Beljonne, J. Cornil, P. Samori, S. Seki and Y. H. Geerts, *Adv. Mater.*, 2016, **28**, 7106-7114.

37. T. J. Aldrich, M. Matta, W. Zhu, S. M. Swick, C. L. Stern, G. C. Schatz, A. Facchetti, F. S. Melkonyan and T. J. Marks, *J. Am. Chem. Soc.*, 2019, **141**, 3274-3287.

38. S. M. Swick, T. Gebraad, L. Jones, B. Fu, T. J. Aldrich, K. L. Kohlstedt, G. C. Schatz, A. Facchetti and T. J. Marks, *Chemphyschem*, 2019, **20**, 2608-2626.

39. H. Huang, L. Yang, A. Facchetti and T. J. Marks, *Chem. Rev.*, 2017, **117**, 10291-10318.

40. N. E. Jackson, B. M. Savoie, K. L. Kohlstedt, M. Olvera de la Cruz, G. C. Schatz, L. X. Chen and M. A. Ratner, *J. Am. Chem. Soc.*, 2013, **135**, 10475-10483.

41. W. Yan, T. Liao, O. Tuguldur, C. Zhong, J. L. Petersen and X. Shi, *Chem. Asian J.*, 2011, **6**, 2720-2724.

42. M. Más-Montoya and R. A. J. Janssen, *Adv. Funct. Mater.*, 2017, **27**, 1605779.

43. N. J. Hestand and F. C. Spano, *Chem. Rev.*, 2018, **118**, 7069-7163.

44. G. Li, X. Zhang, L. O. Jones, J. M. Alzola, S. Mukherjee, L. W. Feng, W. Zhu, C. L.

Stern, W. Huang, J. Yu, V. K. Sangwan, D. M. DeLongchamp, K. L. Kohlstedt, M. R. Wasielewski, M. C. Hersam, G. C. Schatz, A. Facchetti and T. J. Marks, *J. Am. Chem. Soc.*, 2021, **143**, 6123-6139.

45. S. M. Swick, J. M. Alzola, V. K. Sangwan, S. H. Amsterdam, W. Zhu, L. O. Jones, N. Powers-Riggs, A. Facchetti, K. L. Kohlstedt, G. C. Schatz, M. C. Hersam, M. R. Wasielewski and T. J. Marks, *Adv. Energy Mater.*, 2020, **10**, 2000635.
46. R. Wang, C. Zhang, Q. Li, Z. Zhang, X. Wang and M. Xiao, *J. Am. Chem. Soc.*, 2020, **142**, 12751-12759.
47. J. Benduhn, K. Tvingstedt, F. Piersimoni, S. Ullbrich, Y. Fan, M. Tropiano, K. A. McGarry, O. Zeika, M. K. Riede, C. J. Douglas, S. Barlow, S. R. Marder, D. Neher, D. Spoltore and K. Vandewal, *Nat. Energy*, 2017, **2**, 17053-17058.
48. Q. Fan, R. Ma, T. Liu, J. Yu, Y. Xiao, W. Su, G. Cai, Y. Li, W. Peng, T. Guo, Z. Luo, H. Sun, L. Hou, W. Zhu, X. Lu, F. Gao, E. Moons, D. Yu, H. Yan and E. Wang, *Sci. China Chem.*, 2021, **64**, 1380-1388.
49. H. Xu, Y. Yang, C. Zhong, X. Zhan and X. Chen, *J. Mater. Chem. A*, 2018, **6**, 6393-6401.
50. W. Gao, M. Zhang, T. Liu, R. Ming, Q. An, K. Wu, D. Xie, Z. Luo, C. Zhong, F. Liu, F. Zhang, H. Yan and C. Yang, *Adv. Mater.*, 2018, **30**, 1800052.

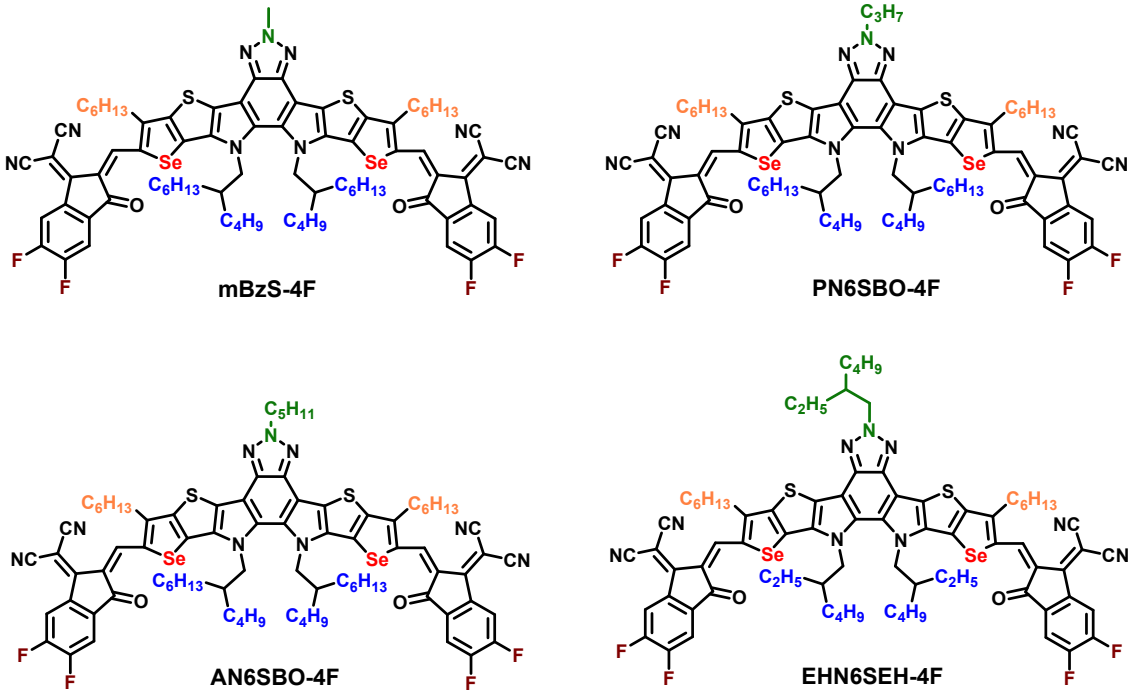

Fig. 1 Molecular structures of the Bz-based NFAs, **mBzS-4F**, **PN6SBO-4F**, **AN6SBO-4F** and **EHN6SEH-4F**.

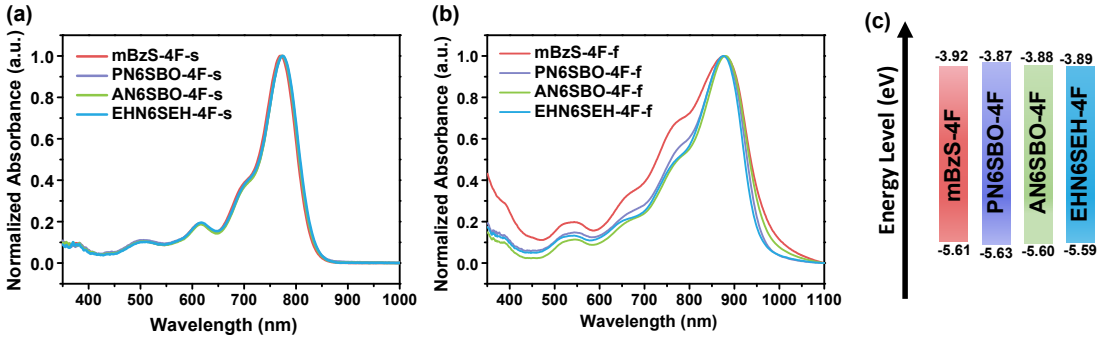

Fig. 2 Normalized UV–vis absorption spectra of **mBzS-4F**, **PN6SBO-4F**, **AN6SBO-4F** and **EHN6SEH-4F** measured as (a) dilute solutions in $CHCl_3$ and (b) thin-films. (c) Frontier orbital energy levels of **mBzS-4F**, **PN6SBO-4F**, **AN6SBO-4F** and **EHN6SEH-4F**.

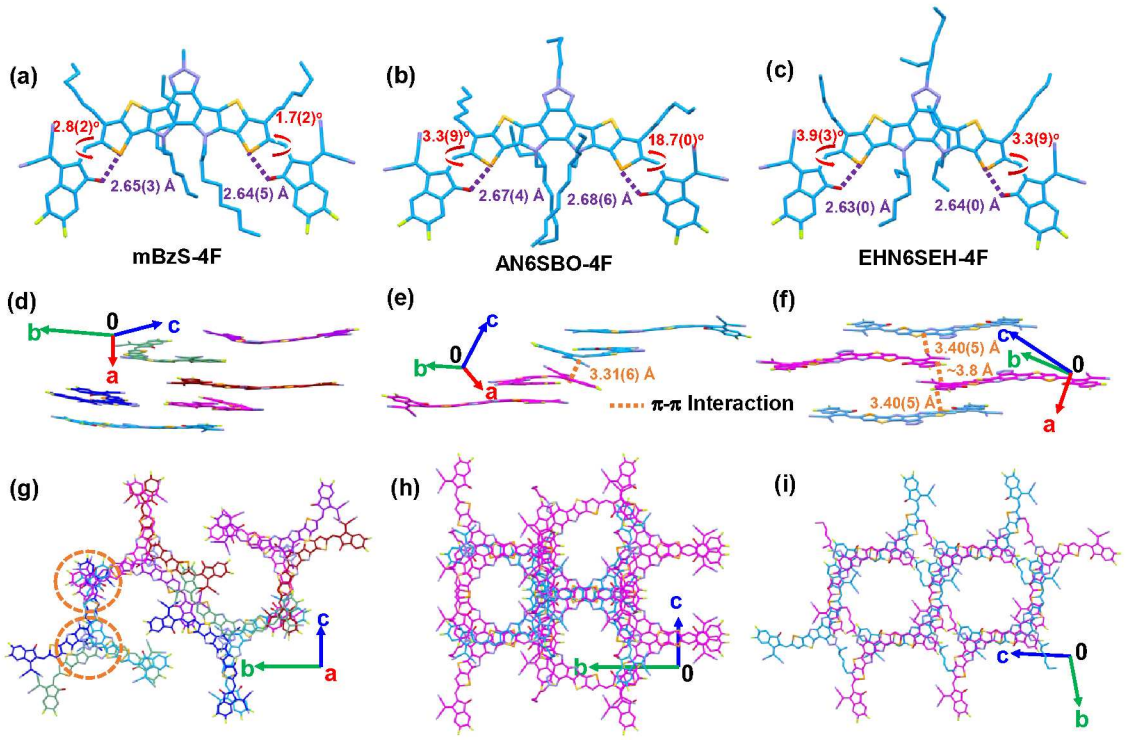

Fig. 3 Single-crystal structures of (a) **mBzS-4F**, (b) **AN6SBO-4F** and (c) **EHN6SEH-4F**. Side view of the molecular packing of (d) **mBzS-4F**, (e) **AN6SBO-4F** and (f) **EHN6SEH-4F**. Top view of the molecular packing of (g) **mBzS-4F**, (h) **AN6SBO-4F** and (i) **EHN6SEH-4F**.

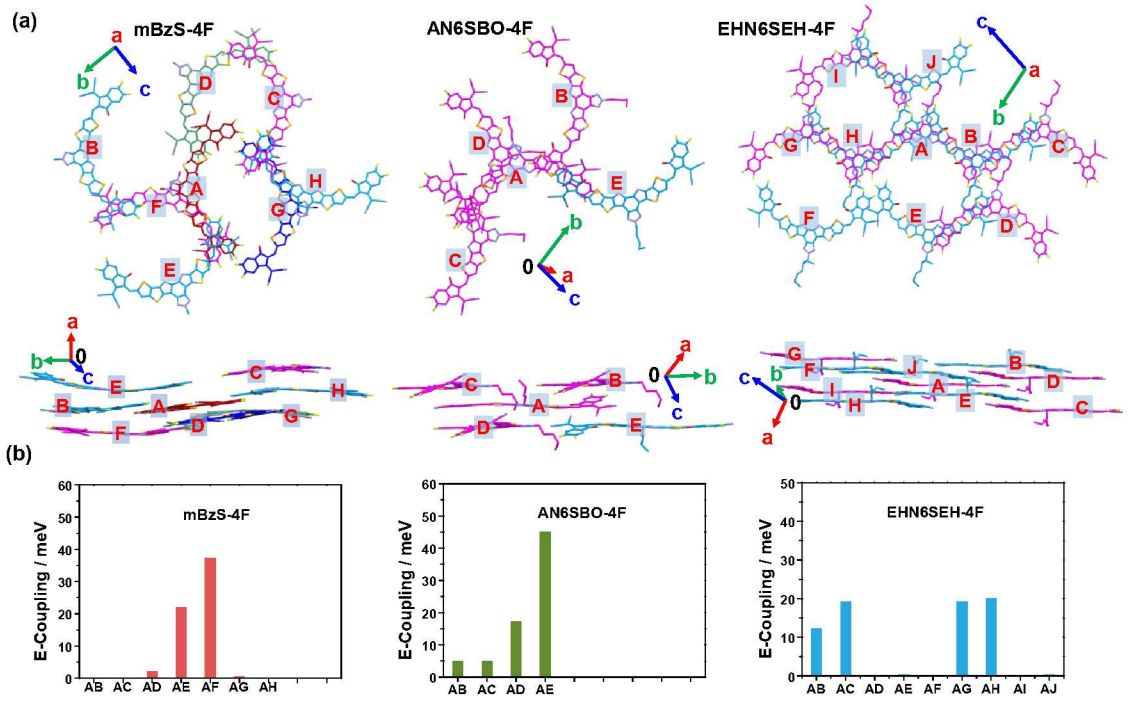

Fig. 4 (a) Top view and side view of the labeled nearest-neighbor molecules in the single-crystal structures of **mBzS-4F**, **AN6SBO-4F** and **EHN6SEH-4F**. (b) Electronic coupling between the nearest neighbors.

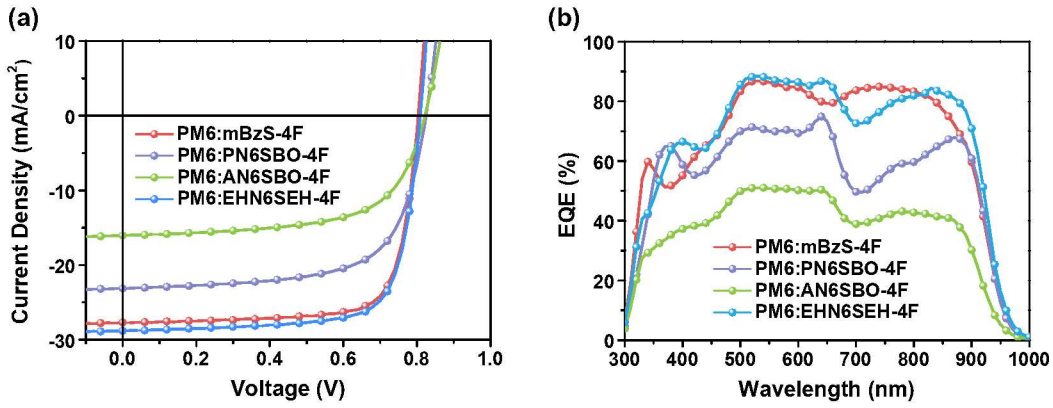

Fig. 5 (a) Solar cell *J*–*V* characteristics. (b) EQE curves of the indicated devices based on PM6:**mBzS-4F**, PM6:**PN6SBO-4F**, PM6:**AN6SBO-4F** and PM6:**EHN6SEH-4F**.

Table 1 Summary of single-crystal parameters of **mBzS-4F**, **AN6SBO-4F** and **EHN6SEH-4F**.

NFAs	Chirality	Color	π-Core Torsion[a]	D-A Dihedral Angle[b]	Se-O Distance	π-π Distance[c]
mBzS-4F	*M*	Azure	13.8(8)°	3.3(5)° / 3.5(9)°	2.56(8) Å / 2.67(9) Å	-
	P	Pink				
	M′	Blue	11.9(8)°	1.1(0)° / 2.9(9)°	2.62(6) Å / 2.69(0) Å	
	P′	Brick Red				
	M″	Green	16.6(5)°	1.7(2)° / 2.8(2)°	2.64(5) Å / 2.65(3) Å	
	P″	Purple				
AN6SBO-4F	*M*	Azure	4.2(2)°	3.3(9)° / 18.7(0)°	2.67(4) Å / 2.68(6) Å	3.31(6) Å
	P	Pink				
EHN6SEH-4F	*M*	Azure	8.6(7)°	3.3(9)° / 3.9(3)°	2.63(0) Å / 2.64(0) Å	3.40(5) Å
	P	Pink				

[a]The π-core torsion was measured by the two planes determined by the selenophene on different side of the core. [b]The D−A dihedral angle was obtained via the two planes built from the adjunct selenophene and the five-membered ring on indanone. [c]The π–π distance was calculated based on the two planes of the five-membered ring of indanone or selenophene on adjacent NFAs.

Table 2 Photovoltaic parameters of the optimized devices based on PM6:**mBzS-4F**, PM6:**PN6SBO-4F**, PM6:**AN6SBO-4F** and PM6:**EHN6SEH-4F** blends.

Blends	V_{oc} (V)	J_{sc} (mA/cm^2)	Integrated J_{sc} (mA/cm^2)	FF (%)	PCE (%)
PM6:**mBzS-4F**	0.804	27.72	27.17	76.35	17.02
PM6:**PN6SBO-4F**	0.825	23.13	22.21	66.65	12.73
PM6:**AN6SBO-4F**	0.822	16.06	15.20	62.98	8.32
PM6:**EHN6SEH-4F**	0.809	28.83	27.80	74.64	17.48

TOC Graphic

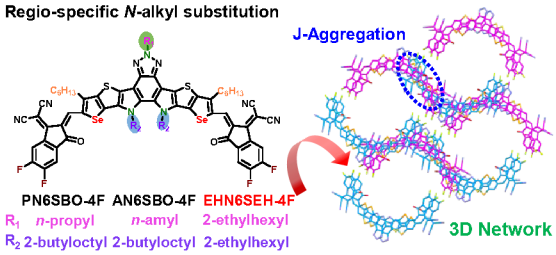
Regio-specific N-alkyl substitution
J-Aggregation
PN6SBO-4F AN6SBO-4F EHN6SEH-4F
R1 n-propyl n-amyl 2-ethylhexyl
R2 2-butyloctyl 2-butyloctyl 2-ethylhexyl
3D Network